Effective viscosity for nematic-liquid-crystal viscosity measurement using a shear horizontal wave

Ryotaro Ozaki,[1] Masashi Aoki,[1] Katsumi Yoshino,[2] Kohji Toda,[3] and Hiroshi Moritake[1]
[1]*Department of Electrical and Electronic Engineering, National Defense Academy, 1-10-20 Hashirimizu, Yokosuka, Kanagawa 239-8686, Japan*
[2]*Shimane Institute for Industrial Technology, 1 Hokuryo-cho, Matsue, Shimane 690-0816, Japan*
[3]*Department of Mechanical Engineering, School of Engineering, Tokyo City University, 1-28-1 Tamazutsumi, Setagaya-ku, Tokyo 158-8577, Japan*
(Received 25 December 2009; revised manuscript received 16 April 2010; published 18 June 2010)

We investigate the effective viscosity of a nematic-liquid-crystal (NLC) for viscosity measurement using a shear horizontal (SH) wave propagating through a glass substrate loaded with the NLC. The phase measurement of the SH wave determines the NLC viscosity because SH wave propagation depends on loaded material viscosity. Using this viscosity measurement, we can also determine the viscosity anisotropy of the NLC with director reorientation. In experiment, phase shifts are detected when voltages are applied to a NLC layer. The measured phases show an unpredictable shift which cannot be explained by conventional director angular dependence of viscosity. To analyze the phase shifts quantitatively, we introduce average effective viscosity for the viscosity measurement using SH wave. This effective viscosity is calculated considering the NLC director configuration and SH wave penetration into the NLC layer. The phase shifts calculated from the effective viscosity well agree with the measured phase shifts. The use of effective viscosity enables quantitative analysis for NLC viscosity measurement using the SH wave and also clarifies the mechanism of the unpredictable SH wave phase shift with director reorientation.

DOI: 10.1103/PhysRevE.81.061703 PACS number(s): 61.30.−v, 66.20.Ej

I. INTRODUCTION

Liquid crystals (LCs) have various anisotropies, such as permittivity, refractive index, and viscosity, owing to their molecular shape. The measurements of such anisotropies are considerable important from both fundamental and practical points of view. In a nematic LC (NLC), there are five independent Leslie viscosity coefficients, which are of practical importance for design of LC displays because display response strongly depends on viscosity [1]. However, the viscosity anisotropy measurement of LCs is not easy compared with the measurement of optical parameters, and various methods have been proposed [2–13]. The anisotropies of the permittivity and refractive index of LCs can be relatively easily determined by capacitance and optical measurements, respectively, using a typical sandwich cell [1]. The viscosity of liquids is generally measured with a rotational viscosity meter. However, this tool is not useful for the anisotropy measurement of an LC because the anisotropy measurement requires a uniform molecular alignment [1,2]. The rotational viscosity meter based on stirring can measure only one average viscosity at a random molecular orientation. Moreover, a relatively large amount of sample is required in the viscosity meter. To resolve these problems, we have demonstrated the use of a shear horizontal (SH) wave for the viscosity measurement of nematic and ferroelectric LCs [7–10].

Acoustic devices have been widely studied for sensor applications [14–21]. It is known that the acoustic devices can measure physical parameters with a small amount of sample. For liquid sensing, an acoustic wave device requires a low-energy loss into a liquid layer. For example, a high propagation loss at a solid/liquid interface occurs in Rayleigh and Lamb wave devices immersed in a viscous liquid because the surface normal component of the acoustic wave radiates into the liquid as a longitudinal wave [22,23]. The SH wave is of particular interest liquid phase application owing to a low-energy loss at a solid/liquid interface. The viscosity of a liquid on a substrate can be determined by measuring the attenuation or phase velocity of the SH wave propagating through the substrate because SH wave propagation is extremely sensitive to change in surface conditions [16–18].

In our system using SH wave, a typical sandwich cell for an NLC is placed at the center of a SH wave delay line. The NLC cell allows to measure viscosity using a small amount of an NLC and to obtain a desired molecular orientation easily by rubbing. The NLC directors can also be controlled by applying a voltage to the cell [8–10]. Although shear waves have been used in NLC viscosity measurements since an early research phase [3–6], our system exhibits some advantages in terms of amount of sample used, control of molecular orientation, and simultaneous measurement of elastic and optical properties [7–10]. However, there is a problem for our method that a conventional propagation analysis for acoustic waves cannot directly adapt to the measurement of the viscosity change in the NLC. This is because the conventional analysis can deal with only a material having a homogeneous viscosity. In the real situation, the viscosity in the NLC layer is not uniform along the thickness direction due to a specific molecular director configuration. Therefore, we have to develop the propagation analysis to consider NLC director configuration.

In this paper, we describe our experiment on SH wave propagation through a glass substrate constituting an NLC cell and then discuss NLC effective viscosity and the phase-shift calculation of the SH wave. The measured phase shifts at low voltages exhibit unpredictable behavior that cannot be explained by conventional director angular dependence of viscosity. However, the calculated phase shifts based on a combination of NLC director calculation, hydromechanics,

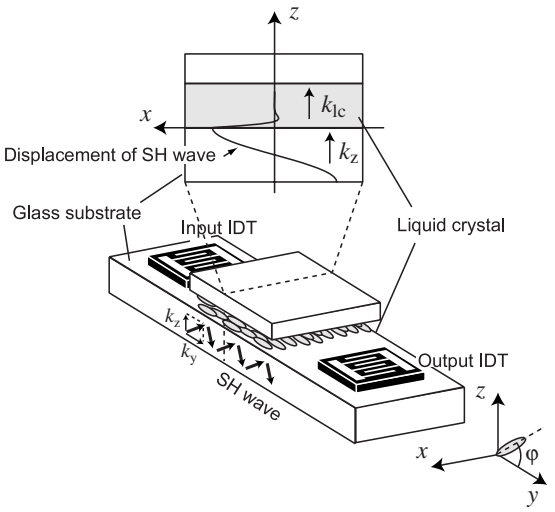

FIG. 1. Schematic of SH wave device with NLC cell for viscosity measurement.

and propagation mode analysis of the SH wave quantitatively agree with the experimental results.

II. BASICS OF VISCOSITY MEASUREMENT USING SH WAVE

In this section, we will discuss the basics of the viscosity measurement using the SH wave. We here consider a SH wave propagating through a thin glass substrate loaded with an NLC, as shown in Fig. 1. The SH wave propagates in the yz plane, and the shear direction is parallel to the x direction. In the glass substrate, the SH wave is confined by reflections at the top and bottom boundaries. At the boundary between the glass and NLC, the SH wave slightly penetrates into the NLC layer. The cross-section view in Fig. 1 illustrates the displacement and penetration of the SH wave. The penetration depending on viscosity causes a phase shift of the SH wave propagation. The measurement of the phase shift at the output interdigital transducer (IDT) determines the viscosity of the liquid crystal on the glass substrate.

We can also detect a phase shift depending on director orientation by applying an electric field to the NLC because the NLC exhibits viscosity anisotropy due to its molecular shape. When an NLC initially orients along the y axis and reorient to the z axis, the shear viscosity η of the NLC is given by

$$\eta(\varphi) = \nu_1 \cos^2 \varphi + \nu_2 \sin^2 \varphi, \tag{1}$$

$$\nu_1 = \frac{1}{2}\alpha_4, \tag{2}$$

$$\nu_2 = \frac{1}{2}\left(\alpha_4 + \alpha_5 - \frac{\alpha_3 + \alpha_2}{\alpha_3 - \alpha_2}\alpha_2\right), \tag{3}$$

where α_i are the Leslie coefficients and φ is the angle between the molecular director and the y axis [1,6]. η is a shear viscosity used for the shear direction perpendicular to the long axis. In other words, the x-direction shear is affected by $\eta(\varphi)$ depending on director angle in the yz plane.

The theoretical phase depending on viscosity can be calculated using propagation mode analysis [24,25]. Let us consider SH wave propagation in the yz plane of the glass substrate with wave vectors k_y and k_z, as shown in Fig. 1. In the glass substrate, the acoustic particle velocity u_g of the SH wave, which represents the shear displacement along the x direction, is given by

$$u_g = \{A_1 \exp(ik_z z) + A_2 \exp(-ik_z z)\}\exp(ik_y y - i\omega t), \tag{4}$$

where A_1 and A_2 are the amplitudes of the SH waves. k_z is written as

$$k_z = \frac{\omega}{u_p}\sqrt{\rho_g \frac{u_p^2}{\mu} - 1}, \tag{5}$$

where u_p is the phase velocity of the SH wave, ρ_g is the mass density of the glass substrate, and μ is the modulus of elasticity in shear of the glass substrate.

The flow velocity u_{lc} of the SH wave in the NLC layer is obtained using the Navier-Stokes equation

$$\frac{\partial u_{lc}}{\partial t} = \frac{1}{\rho_{lc}}\frac{\partial}{\partial z}\left(\eta\frac{\partial u_{lc}}{\partial z}\right), \tag{6}$$

where ρ_{lc} and η are the mass density and viscosity of the NLC, respectively. We here regard the NLC as an incompressible fluid. When η is spatially uniform, the solution u_{lc} is given by

$$u_{lc} = A_3 \exp(-k_{lc} z)\exp(ik_z z - i\omega t), \tag{7}$$

where A_3 is the amplitude of the SH wave that penetrated into the NLC layer and k_{lc} is the wave vector of the SH wave. Equation (7) denotes the flow velocity that exponentially decays with $\exp(-k_{lc}z)$ in the NLC layer, where k_{lc} is written as

$$k_{lc} = \sqrt{\frac{\omega\rho_{lc}}{2\eta}}. \tag{8}$$

For propagation mode analysis, stresses in the glass substrate and NLC are also necessary. In the glass substrate, the relation between the stress T_g and the acoustic particle velocity u_g is given by

$$\frac{\partial T_g}{\partial t} = \mu\frac{\partial u_g}{\partial z}, \tag{9}$$

while the shear stress in the NLC layer is written as

$$T_{lc} = \eta\frac{\partial u_{lc}}{\partial z}. \tag{10}$$

The boundary conditions of the velocities and stresses along the z axis are summarized as

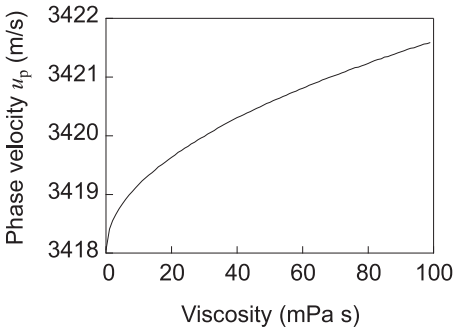

FIG. 2. Viscosity dependence of phase velocity for first-mode SH wave in glass substrate load with viscous fluid.

$$\begin{bmatrix} \mu k_z & -\mu k_z & -(i-1)\omega\eta k_{lc} \\ \exp(-ik_z D) & -\exp(ik_z D) & 0 \\ 1 & 1 & -1 \end{bmatrix} \begin{bmatrix} A_1 \\ A_2 \\ A_3 \end{bmatrix} = 0, \tag{11}$$

where D is the thickness of the glass substrate. The wave vector k_z including u_p is determined by solving Eq. (11). Figure 2 shows the viscosity dependence of u_p. Here, we calculated it using the following experimental parameters: μ of 2.64×10^{10} N/m^2, ρ_g of 2760 kg/m^3, ρ_{lc} of 1019 kg/m^3, D of 400 μm, and f of 9.1 MHz. Details of the experimental conditions and procedure are described in the next section. As is evident in Fig. 2, phase velocity increases with increasing viscosity and is proportional to the square root of viscosity. Note that the propagation phase of the SH wave is linked to viscosity. Using this relation, we can determine the viscosity of the NLC on the glass substrate by measuring phase propagation.

III. EXPERIMENT

A. Experimental procedure

We fabricated SH wave devices shown in Fig. 1 to measure phase propagation depending on viscosity. An NLC cell structure was prepared at the center to be filled with a measurement sample; the cell length along the y axis was 1.5 cm. The cell length corresponds to the propagation length of the NLC delay line for the SH wave. The cell consisted of two indium-tin oxide (ITO)-coated glass substrates sandwiching two poly(ethylene terephthalate) films of 32 μm thickness as a spacer. The surface of the ITO glasses were coated with polyimide (JSR, AL1254) and unidirectionally rubbed along the y axis. The test sample was 4-cyano-4′-pentylbiphenyl (5CB), which is a typical NLC. Figure 3 shows schematic views of director configuration with or without an electric field. In the cell, the NLC molecules were aligned along the y axis in the absence of an electric field. The molecules were then reoriented to the z axis upon application of an electric field to the ITO electrodes.

On both sides of the NLC cell, two piezoelectric ceramic plates (TDK, 101A) were placed for SH wave excitation and detection, as shown in Fig. 1. The thickness of the glass substrate and piezoelectric plate were 400 μm and 1 mm,

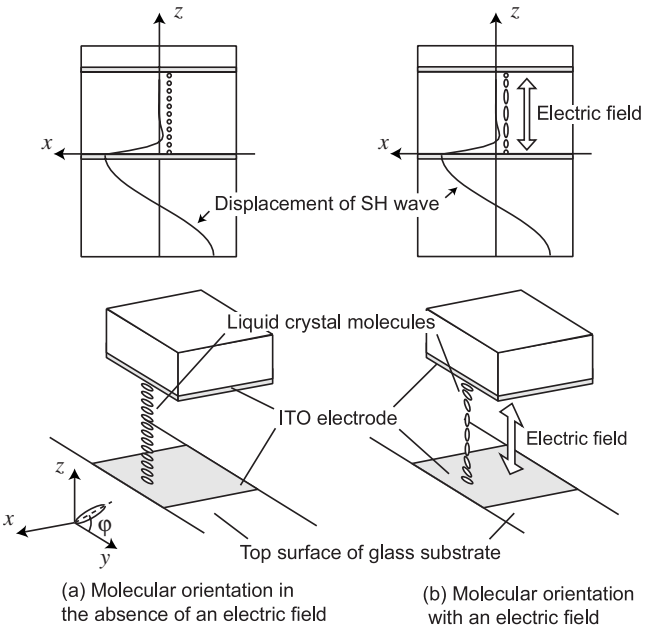

FIG. 3. Schematic views of NLC director configuration with or without an electric field.

respectively. IDTs were prepared on the piezoelectric ceramic plates by aluminum evaporation. The periodicity of the IDT was 400 μm, and the number of the pairs of electrode fingers was 7. To excite SH wave, a sinusoidal voltage of 3 V was applied to the input IDT. Since the piezoelectric ceramic plates were polarized along the x axis, the SH wave shear direction excited from the piezoelectric plates was parallel to the x axis. The SH wave excited from the input IDT propagated through the lower glass plate in contact with the NLC, and then the signal was detected by the output IDT. To detect the SH wave phase shift, the output IDT was connected to a lock-in amplifier (Stanford Research System, SR844). All measurements were performed at 20 °C in a temperature controller.

B. Experimental results

Figure 4 shows the frequency dependence of the insertion loss in the SH wave device. Peaks in Fig. 4 correspond to mode frequencies for the SH wave propagating in the glass

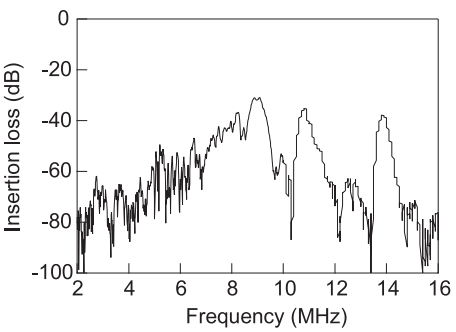

FIG. 4. Frequency dependence of insertion loss of SH wave device. Peaks correspond to propagation mode frequencies.

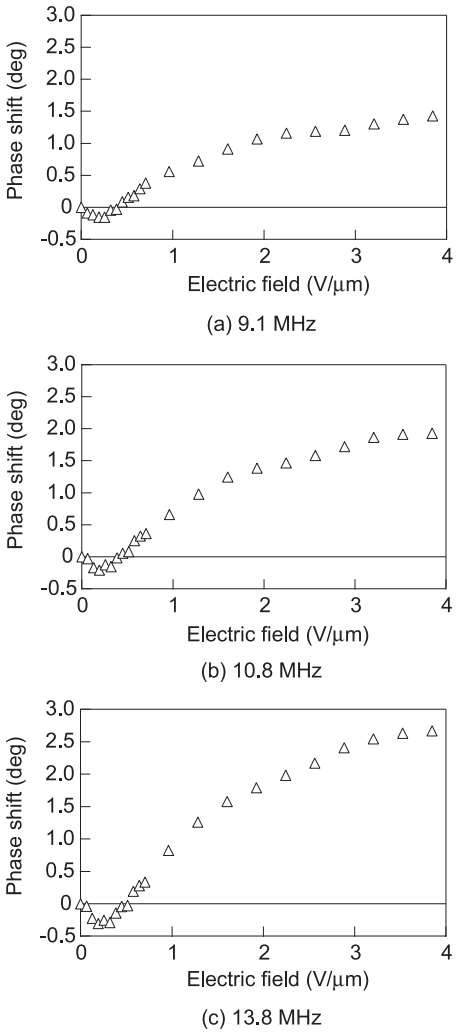

FIG. 5. Electric field dependences of SH wave phase shift for first-, second- and third-mode frequencies.

plate. The frequencies of the first, second, and third modes are 9.1, 10.8, and 13.8 MHz, respectively, at which we measured the phases of the SH wave for various applied electric fields. The phase θ is defined as

$$\theta = \omega L/u_p, \tag{12}$$

where L is the NLC delay line length. Since u_p depends on viscosity as shown in Fig. 2, θ also has viscosity dependence. A larger u_p means a larger viscosity, hence a decrease in θ indicates an increase in viscosity. Figure 5 shows the electric field dependences of relative phase shift in the SH wave which detected at the output IDT. The phase shifts were determined from the difference from the phase at 0 V as a criterion; $\Delta\theta = \theta(V) - \theta_{0V}$. As is evident in Fig. 5, the phase shift increases with increasing frequency. This can be explained by the fact that phase is proportional to frequency as shown in Eq. (12). At each frequency, the phases decrease at low electric fields and then increase with increasing electric field. Here, the NLC directors were reoriented from the y axis to the z axis with increasing electric field, as shown in Fig. 3. Since phase decreases with increasing viscosity, the measured phase shifts imply that viscosity slightly increases at low electric fields and then it decreases at high electric fields.

TABLE I. Leslie viscosity coefficients of 5CB.

Viscosity coefficient	mPa s
α_1	−11
α_2	−70
α_3	−4
α_4	71
α_5	52
α_6	−28

To discuss the viscosity change, we calculated the director angular dependence of shear viscosity using Eq. (1) with the Leslie coefficients for 5CB listed in Table I [26]. The calculated director angular dependence of shear viscosity for 5CB is shown in Fig. 6. In our experimental configuration, the initial shear viscosity is $\eta(0°) = 35.5$ mPa s at 0 V, and then it decreases toward $\eta(90°) = 22.5$ mPa s with director reorientation. As is evident in Fig. 6, in theory, the viscosity of 5CB monotonically decreases with increasing director angle. That is, the director reorientation toward the z axis with an electric field causes an increase in phase shift owing to decreasing viscosity. Actually, in Fig. 5, the measured phase shifts increase with increasing electric field at higher than 0.25 V/μm. With the exception of low electric fields less than 0.25 V/μm, we can qualitatively explain the profile of phase shift by the director angular dependence of viscosity. However, the measured phase shifts show a decrease in phase at the low electric fields in spite of increasing director angle from 0°. The dip at the low electric fields is not an experimental error because every sample shows the same behavior. We cannot explain why viscosity increases at the low electric fields because the viscosity for the initial orientation should be maximum in our configuration. The results in Fig. 5 contradict the expected behavior from the model of Eq. (1). We also cannot explain the phase shift quantitatively using the model. The measured phase shift at 4 V/μm for 9.1 MHz is +1.4°. However, when NLC viscosity changes from $\eta(0°) = 35.5$ mPa s to $\eta(90°) = 22.5$ mPa s, the estimated phase shift from Fig. 2 and Eq. (12) is about +2.1°. If

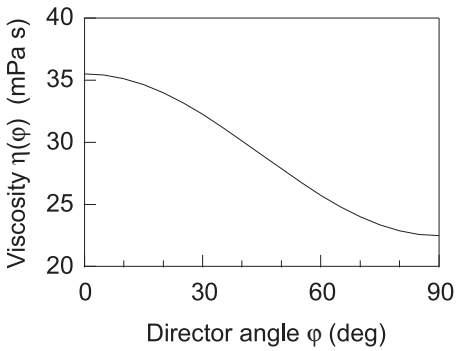

FIG. 6. Shear viscosity for 5CB as a function of director angle φ.

the NLC directors reorient from $\varphi=0°$ to $\varphi=90°$, the measured value is quite smaller than the estimated value. In addition, we also cannot explain why the phase still increased from 3 to 4 V/μm. For the 32-μm-thick cell, 3 and 4 V/μm are 96 and 128 V, respectively. Such high voltages are sufficient to reorient directors along the z axis.

We have considered that these problems are caused by the use of the model in Sec. II that is assumed a spatially uniform director along the z direction. In the real situation, this is not the case, and therefore a modification to the model must be made. Recently, we have answered the above questions from a phase-shift calculation considering NLC director configuration, penetration depth, and propagation mode of the SH wave. Our modifications and explanations will be given in the next section.

IV. CALCULATION AND DISCUSSION

A. Effective viscosity

The SH wave propagation in the device is affected by the director configuration in the NLC layer. To understand the propagation characteristics, the interaction between the NLC and SH wave has to be clarified. The keys to do this are the director configuration and the penetration depth of the SH wave because the director configuration in the NLC layer is not spatially uniform. The NLC director configuration can be calculated using Frank's continuum theory [1,27]. In our case, the free energy density g for NLC is given by

$$g = \frac{1}{2}K_{11}(\nabla \cdot \mathbf{n})^2 + \frac{1}{2}K_{33}\{\mathbf{n} \times (\nabla \times \mathbf{n})\}^2 - \frac{1}{2}\varepsilon_0\varepsilon_a(\mathbf{E} \cdot \mathbf{n})^2, \tag{13}$$

where K_{11} and K_{33} are the splay and bend elastic constants, respectively, $\boldsymbol{n}$ is the director vector of a molecule, ε_a is the anisotropy of dielectric constant, and $\boldsymbol{E}$ is the electric field. Using the director angle φ, g is written as

$$g = \frac{1}{2}\left\{(K_{11}\cos^2\varphi + K_{33}\sin^2\varphi)\left(\frac{d\varphi}{dz}\right)^2 - \varepsilon_0\varepsilon_a E^2 \sin^2\varphi\right\}. \tag{14}$$

The director configuration can be obtained by substituting g into the Euler-Lagrange equation.

Figure 7 shows director configurations in the NLC layer for various electric fields. In this calculation, we assumed that the pretilt angle of the NLC is 1.5° and that the boundary condition is strong anchoring. K_{11}, K_{33}, and ε_a for 5CB are 6.4 pN, 8.6 pN, and 11.0, respectively. The director angles gradually increase with increasing electric field and form an arched curve. Almost all of the directors redirect to 90° at 1 V/μm. Note that director angle continuously changes near the boundary owing to strong anchoring. This represents that the molecules on the surfaces are strongly anchored to the polyimide alignment film and that the other molecules are redirected toward the z axis by the electric field. The schematic illustration of the director distribution with the strong anchoring is shown in Fig. 3(b). In the NLC layer, this continuous angle change leads to a continuous

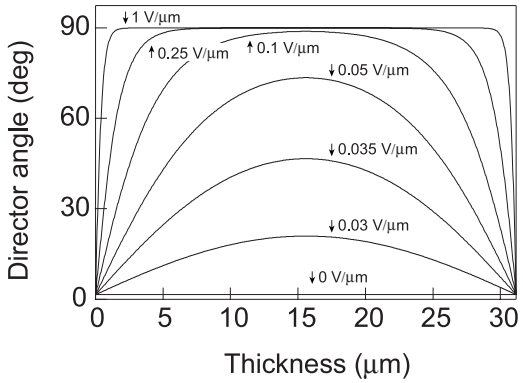

FIG. 7. Calculated director configurations in 32-μm-thick cell for various electric fields.

viscosity change. Since the SH wave penetrates and mainly exists in the vicinity of the boundary, the SH wave propagation is strongly affected by the viscosity change near the boundary. Figure 8 shows the viscosity distributions obtained by substituting the calculated director angles into Eq. (1). The viscosity linked to the director angle decreases from the center of the cell with increasing electric field. In contrast, the viscosity at the boundary does not change owing to the strong anchoring.

We consider that the SH wave propagating in the device is affected by an effective viscosity which is an average value taking into account the viscosity distribution and SH wave penetration. The penetration of the SH wave into the NLC layer can be calculated using the Navier-Stokes equation [Eq. (6)]. When viscosity is constant in the layer, the flow velocity of the SH wave is expressed by Eq. (7). However, since the viscosity in the NLC layer is not spatially uniform owing to the director configuration, we have to calculate the Navier-Stokes equation numerically using a differential method. Figure 9 shows the calculated flow velocities of the SH waves in the NLC layer for electric fields of 0 and 1 V/μm. The SH waves exponentially decay in the NLC layer, and the $1/e$ lengths as penetration depths for 0 and 1 V/μm are 0.79 and 0.73 μm, respectively. The penetration depth for 1 V/μm is shorter than that for 0 V/μm

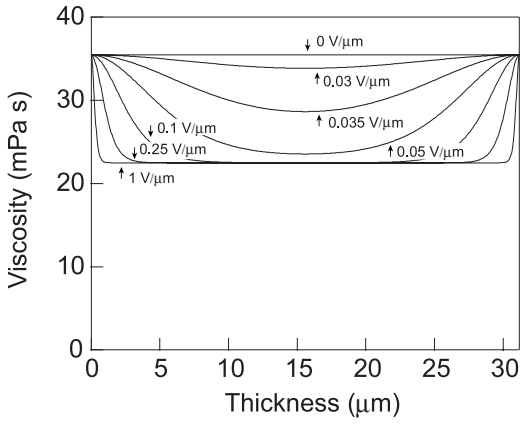

FIG. 8. Viscosity distributions in 32-μm-thick cell for various electric fields. These are calculated using director configurations in Fig. 7.

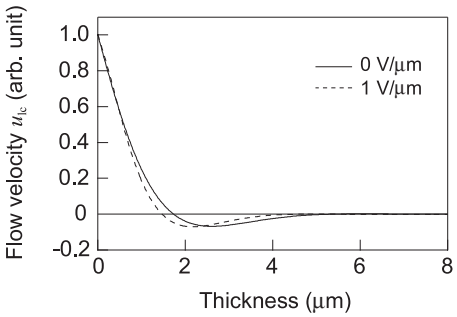

FIG. 9. Flow velocities of SH wave in NLC layer for applied electric fields of 0 and 1 $V/\mu m$.

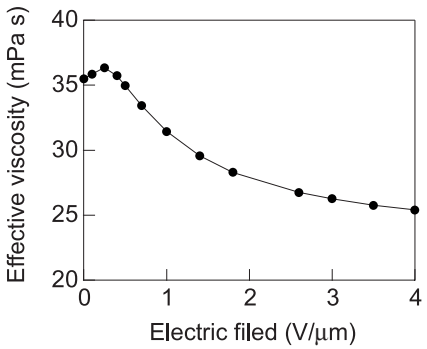

FIG. 10. Calculated effective viscosity in NLC layer for SH wave of 9.1 MHz as function of electric field.

because the viscosity for 1 $V/\mu m$ is lower as shown in Fig. 8.

To determine average effective viscosity, we discuss mechanical work W done by the SH wave on the NLC. W can be obtained by integrating power over time:

$$W = \int u_{lc} \eta \frac{\partial u_{lc}}{\partial z} dt. \tag{15}$$

Here, we deal with two types of mechanical work: one is W considering an NLC viscosity distribution and other is W' not considering the viscosity distribution. Assuming that an NLC has an effective viscosity η_{eff}, the NLC can be treated as a homogeneous material. When viscosity is uniform, W' is written by

$$W'(z) = \frac{1}{\sqrt{2}} \eta_{\text{eff}} \frac{k}{\omega} A^2 \exp(-2kz)\cos(2kz), \tag{16}$$

where power is integrated over a half period of time and a constant term is ignored to investigate work caused by periodic flow. In contrast, when we perform a calculation considering the viscosity distribution, W has to be computed Eq. (15) using finite differential method. The two works should be equal:

$$\int_0^D W'(z)dz = \int_0^D W(z)dz. \tag{17}$$

Using this relation, η_{eff} is written as

$$\eta_{\text{eff}} = \frac{\int_0^D W(z)dz}{\frac{1}{\sqrt{2}} \frac{k}{\omega} A^2 \int_0^D \exp(-2kz)\cos(2kz)dz}. \tag{18}$$

Figure 10 shows the calculated effective viscosity for the SH wave of 9.1 MHz as a function of applied electric field, which is obtained from Eq. (18). The calculated effective viscosity slightly increases at low voltages and then decreases with increasing electric field. Note that this characteristic is quite similar to the experimental results of the SH wave phase shift. The measured phases in Fig. 5 decrease at low electric fields and then increase with increasing electric field. As mentioned before, the phase shift indicates that viscosity increases at low electric fields and then decreases. That is, the applied electric field dependence of effective viscosity is consistent with the experimental results.

B. Comparison of calculation and experimental results

We calculated effective viscosity by taking into account the director configuration, SH wave penetration depth, and mechanical work in the NLC layer. The electric field dependence of effective viscosity qualitatively agreed with that of the measured phase shift. To quantitatively verify the effective viscosity, we calculated the phase shifts using Eqs. (11) and (12). The measured and calculated phase shifts for each frequency are shown in Fig. 11. Here, the measured phase shifts are the same with the results shown in Fig. 5. The experimental results were again plotted to compare with the calculated phase shifts. As is evident in Fig. 11, the calculated phase shifts well agree with the measured phase shifts. Both measured and calculated results show a slight decrease in phase at low electric fields, and then the phase gradually increases with increasing electric field. In addition, the calculated phase shifts are consistent with the measured results for each frequency. This means that the frequency dependence of the phase shift is also calculated correctly.

Interestingly, despite the fact that the NLC viscosity is the highest at 0° as shown in Fig. 4, our experiment and calculation show the highest viscosity when the directors are slightly tilted from 0° at low electric fields. We finally figured out the reason for such an interesting behavior by the effective viscosity calculation. This can be explained by the relation between the viscosity distribution and the direction of mechanical work in the NLC layer. Here, we again discuss mechanical work W done by the SH wave on the NLC. To explain clearly the behavior, the viscosity and other components of W are separately plotted in Fig. 12. The solid lines show the product of the flow velocity and its partial differentiation, and the dotted lines show viscosity that is the same data in Fig. 8. Note that the solid lines have positive or negative values. The sign denotes the direction of work. That is, we have to consider the flow direction of the SH wave in the NLC layer. In this case, the direction of the work in the negative region at approximately 1 μm is opposite that at the top of the glass substrate ($z=0$). According to Eq. (15), the product of the solid and dotted lines is equal to mechanical work. In Fig. 12(a), the viscosity distribution is flat in the

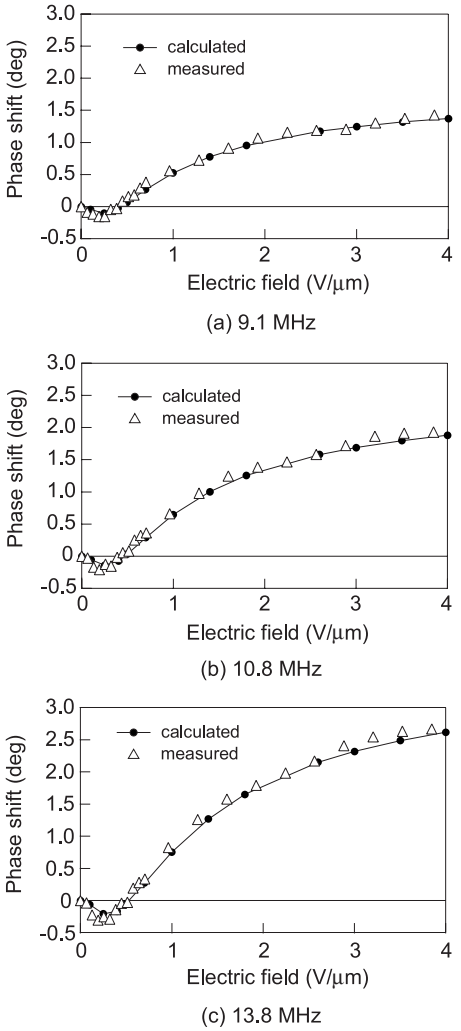

FIG. 11. Electric field dependences of measured and calculated phase shifts for SH waves of 9.1, 10.8, and 13.8 MHz.

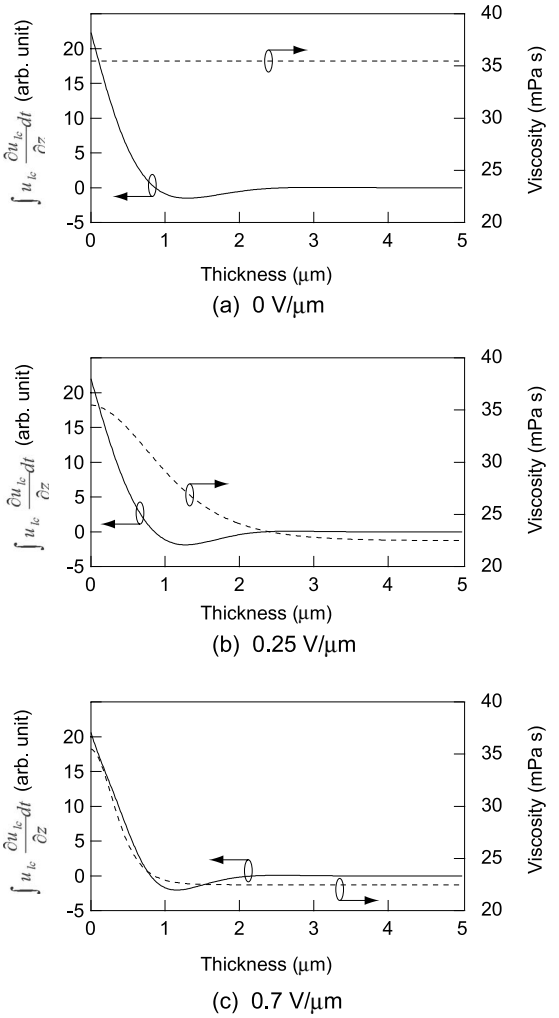

FIG. 12. Viscosity distributions and integrals of product of flow velocity and its partial differentiation over a half period of time in vicinity of boundary between glass substrate and NLC layer. These are components of the mechanical work written in Eq. (18).

NLC layer because all the NLC molecules are directed to 0° as the initial orientation. Here, we regarded the work at 0 V/μm as a criterion. In Fig. 12(b), viscosity gradually decreases in the NLC layer, and the viscosity distribution for 0.25 V/μm is not uniform any more. Considering total work that is an integration of W over the NLC layer, the total work for 0.25 V/μm becomes larger than that for 0 V/μm because viscosity mainly decreases in the negative region of the solid line and slightly decreases in the positive region of the solid line in the vicinity of the glass surface. That is, the total work at 0.25 V/μm relatively increases compared with that at 0 V/μm. On the other hand, at 0.7 V/μm, viscosity decreases in wider areas including the positive region near the glass surface, as shown in Fig. 12(c). As a result, the total work decreases at high electric fields. Since total work is proportional to effective viscosity as shown in Eq. (18), we can explain the reason for the effective viscosity change in Fig. 10. Thus, the effective viscosity of the NLC could be calculated from the mechanical work done by the SH wave on the NLC. Furthermore, the increase in viscosity at the low electric fields could also be explained by considering the flow direction of the SH wave.

V. CONCLUSIONS

We examined the SH wave phase shift to develop a viscosity measurement process for NLCs. Although a monotonic increase in phase shift was expected owing to the simple decrease in viscosity with director reorientation, the experimental results showed an unexpected shift that had a slight decrease in phase at low electric fields and a large increase in phase at high electric fields. To investigate the phase shift, we considered the average effective viscosity of an NLC layer for the SH wave. The effective viscosity was calculated by taking into account the NLC director configuration, SH wave penetration depth, and mechanical work done by the SH wave on the NLC. We then performed propagation mode analysis of the SH wave using the effective viscosity to obtain the phase shift. The calculated phase shifts quantitatively agreed with the measured phase shifts. Furthermore, the frequency dependence of the phase shift also agreed with the experimental results. These support the notion that our introduced effective viscosity is appropriate

for NLC viscosity measurement using the SH wave. We also successfully clarified the mechanism of the electric field dependence of the phase shift. We consider that phase-shift analysis is very useful for the viscosity measurement of NLCs.

ACKNOWLEDGMENT

The authors would like to acknowledge the helpful discussion with Professor Yabushita of the National Defense Academy of Japan.

[1] P. G. de Gennes and J. Prost, *The Physics of Liquid Crystals*, 2nd ed. (Oxford Science, Oxford, 1993).
[2] M. Miesowicz, Nature (London) **158**, 27 (1946).
[3] P. Martinoty and S. Candau, Mol. Cryst. Liq. Cryst. **14**, 243 (1971).
[4] H. Nakamura, Y. Naito, Y. Tsuboi, S. Mitaku, and K. Okano, Jpn. J. Appl. Phys. **21**, 1539 (1982).
[5] Y. Kawamura and K. Okano, Jpn. J. Appl. Phys. **22**, L730 (1983).
[6] Y. Kawamura and K. Okano, Jpn. J. Appl. Phys. **22**, 1749 (1983).
[7] M. Inoue, H. Moritake, K. Toda, and K. Yoshino, Jpn. J. Appl. Phys. **39**, 5632 (2000).
[8] M. Inoue, K. Yoshino, H. Moritake, and K. Toda, Appl. Phys. Lett. **79**, 4345 (2001).
[9] M. Inoue, K. Yoshino, H. Moritake, and K. Toda, J. Appl. Phys. **91**, 2798 (2002).
[10] R. Ozaki, M. Aoki, K. Yoshino, K. Toda, and H. Moritake, Jpn. J. Appl. Phys. **46**, 4734 (2007).
[11] Y. Kuratomi, T. Miyashita, T. Kishimoto, T. Ishinabe, and T. Uchida, *Proceedings of the 12th International Display Workshops* (ITE, Tokyo, 2005), p. 45.
[12] N. Murazawa, S. Juodkazis, V. Jarutis, Y. Tanamura, and H. Misawa, Europhys. Lett. **73**, 800 (2006).
[13] Y. Iwata, H. Naito, M. Inoue, H. Ichinose, M. Klasen-Memmer, and K. Tarumi, Thin Solid Films **517**, 1421 (2008).
[14] H. Wohltjen and R. Dessy, Anal. Chem. **51**, 1458 (1979).
[15] T. Moriizumi, Y. Unno, and S. Shiokawa, *Proceedings of the IEEE US Symposium* (IEEE, New York, 1987), p. 579.
[16] A. J. Ricco and S. J. Martin, Appl. Phys. Lett. **50**, 1474 (1987).
[17] T. M. Niemczyk, S. J. Martin, C. G. Frye, and A. J. Ricco, J. Appl. Phys. **64**, 5002 (1988).
[18] F. Josse and Z. Shana, J. Acoust. Soc. Am. **84**, 978 (1988).
[19] M. Castaings and P. Cawley, J. Acoust. Soc. Am. **100**, 3070 (1996).
[20] F. Bender, R. Dahint, and F. Josse, IEEE Trans. Ultrason. Ferroelectr. Freq. Control **46**, 1497 (1999).
[21] R. Lucklum, C. Behling, and P. Hauptmann, IEEE Trans. Ultrason. Ferroelectr. Freq. Control **47**, 1246 (2000).
[22] F. Josse and Z. Shana, J. Acoust. Soc. Am. **85**, 1556 (1989).
[23] A. Sawaguchi and K. Toda, Jpn. J. Appl. Phys. **31**, 3094 (1992).
[24] J. J. Campbell and W. R. Jones, IEEE Trans. Sonics Ultrason. **15**, 209 (1968).
[25] G. W. Farnell, IEEE Trans. Sonics Ultrason. **17**, 229 (1970).
[26] K. Negita, J. Chem. Phys. **105**, 7837 (1996).
[27] F. C. Frank, Discuss. Faraday Soc. **25**, 19 (1958).